

Molecular docking of substrates and inhibitors in the catalytic site of CYP6B1, an insect cytochrome P450 monooxygenase

Jerome Baudry¹, Weimin Li², Liping Pan²,
May R. Berenbaum³ and Mary A. Schuler^{2,4}

¹School of Chemical Sciences, ²Department of Entomology and
³Department of Cell and Structural Biology, University of Illinois at
Urbana-Champaign, 190 ERML, 1201 West Gregory Drive, Urbana,
IL 61801, USA

⁴To whom correspondence should be addressed.
E-mail: maryschu@uiuc.edu

Furanocoumarins represent plant toxins that are used in the treatment of a variety of skin diseases and are metabolized by cytochrome P450 monooxygenases (P450s) existing in insects such as *Papilio polyxenes* (the black swallowtail). To elucidate the active site in the CYP6B1 protein that is the principal P450 existing in this species, we have constructed a homology model of it based on sequence and structure alignments with the bacterial CYP102 protein whose crystal structure has been defined and with the insect CYP6B4 protein that also metabolizes furanocoumarins. In the derived CYP6B1 model, Phe116 and His117 in SRS1, Phe371 in SRS5 and Phe484 in SRS6 contribute to the formation of a resonant network that stabilizes the P450's catalytic site and allows for interactions with its furanocoumarin substrates. The first two of these residues are absolutely conserved in all members of the insect CYP6B subfamily and the last two are variable in different members of the CYP6B subfamily. A combination of theoretical and experimental docking analyses of two substrates (xanthotoxin and bergapten) and two inhibitors (coumarin and pilocarpine) of this P450 provide significant information on the positioning of furanocoumarins within this catalytic pocket. Molecular replacement models based on the results of variations at two of these critical amino acids provide support for our furanocoumarin-docked model and begin to rationalize the altered substrate reactivities observed in experimental analyses.

Keywords: furanocoumarin metabolism/homology modeling/
P450 monooxygenases/substrate docking

Introduction

Furanocoumarins represent natural products present in over a dozen plant families and many foodstuffs including celery, parsley, figs, parsnips and grapefruit juice (Anderson and Voorhees, 1980; Berenbaum, 1991; Fukuda *et al.*, 1997; Schmiedlin-Ren *et al.*, 1997) that are extremely phototoxic to a wide variety of prokaryotic and eukaryotic organisms (Berenbaum, 1991). Two types of furanocoumarins exist: linear forms with their furan rings attached to the 6 and 7 positions of the coumarin nucleus and angular forms with their furan rings attached to the 7 and 8 positions of the coumarin nucleus. One aspect of their toxicity results from the ability of

UV-A photoactivated furanocoumarins to react directly with pyrimidine nucleotides forming mono- and di-adducts in DNA (Berenbaum, 1991). Another aspect of their toxicity derives from the ability of UV-A-photoactivated furanocoumarins to react with ground state oxygen generating toxic oxyradicals capable of globally inactivating proteins within cells. The photobiological reactivities of furanocoumarins with DNA allow them to serve as naturally occurring insecticides and feeding deterrents for herbivorous insects and livestock, some of which encounter high doses of these toxins in their diets (Berenbaum, 1991). These reactivities have also allowed them to be developed as pharmaceuticals for a wide range of therapeutic applications (vitiligo, psoriasis, skin cancers) requiring cell division inhibitors. Three of the most common naturally occurring linear furanocoumarins used for these purposes are xanthotoxin, bergapten and psoralen. The last remaining aspect of their toxicity and the one which can lead to severe problems with drug–drug interactions (Guengerich, 1997; Lin and Lu, 1998) is their ability to competitively and/or mechanistically inhibit a variety of human P450s, including CYP1A2 (Mays *et al.*, 1987; Apseloff *et al.*, 1990; Ono *et al.*, 1996), CYP2A6 (Ono *et al.*, 1996; Draper *et al.*, 1997; Koenigs *et al.*, 1997; Koenigs and Trager, 1998; Zhang *et al.*, 2001) and CYP3A4/5 (Ameer and Weintraub, 1997; Lown *et al.*, 1997; Schmiedlin-Ren *et al.*, 1997; Guo *et al.*, 2000a,b). Despite their wide use as pharmaceuticals and the presence of these compounds in the diets of humans and other herbivores, catalytic site residues critical for furanocoumarin metabolism and/or interaction with inhibitors have not yet been defined for any of these vertebrate P450s.

In comparison with mammalian P450s, insect P450s have only recently been defined despite the enormous importance of these monooxygenases in the metabolism of endogenous (hormones and pheromones) and exogenous (insecticides and plant toxins) substances. Among the best characterized of the insect P450s is the CYP6B1 protein expressed in the guts of *Papilio polyxenes* (black swallowtail caterpillar) larvae (Cohen *et al.*, 1992; Hung *et al.*, 1995). Cloning and heterologous expression of this protein using recombinant baculovirus vectors has demonstrated that the CYP6B1 protein is capable of metabolizing a wide range of linear furanocoumarins encountered in the diet of this insect but not appreciable amounts of angular furanocoumarins (Ma *et al.*, 1994; Hung *et al.*, 1997; Chen *et al.*, 2002). Additional members of the CYP6B subfamily of monooxygenases existing in *Papilio glaucus* (tiger swallowtail) and *Helicoverpa zea* (corn earworm) share extensive amino acid identity with CYP6B1 (53–63%) and at least some share furanocoumarin metabolic capabilities (Hung *et al.*, 1997; Li *et al.*, 2000, 2002a, 2003). Comparisons between these various CYP6B subfamily members have indicated that they are unusually well conserved in variable substrate recognition site (SRS) regions that contribute to the evolution and divergence of other P450 proteins (Gotoh,

1992; Berenbaum *et al.*, 1996). Specifically, 24 of 34 amino acids, including Phe116 and His117 in the SRS1 region, are absolutely conserved among all *CYP6B* subfamily members currently known (Cohen *et al.*, 1992; Hung *et al.*, 1995; Berenbaum *et al.*, 1996; Li *et al.*, 2000, 2002a,b). Other positions such as Ala113 and Ile115 just upstream of these conserved amino acids in SRS1 and the entire SRS6 region near the C-terminus of this protein are considerably more variable in different members of the *CYP6B* subfamily. Site-directed mutagenesis of the conserved Phe116 and His117 in the SRS1 region and the variable Phe484 in the SRS6 region, based on a first stage model for this P450, have indicated that aromatic amino acids in both SRS1 and SRS6 are essential for proper folding of the catalytic site and for defining the range of substrates metabolized (Chen *et al.*, 2002). Even so, the nature of the side chain interactions stabilizing this catalytic site and the protein–substrate interactions facilitating efficient furanocoumarin metabolism by this P450 were not evident.

This and other analyses identifying amino acids within SRS1 in the *CYP2A* (Lindberg and Negishi, 1989; Negishi *et al.*, 1996), *CYP2B* (Szklarz *et al.*, 1995; von Wachenfeldt and Johnson, 1995; Domanski *et al.*, 1999), *CYP2C* (Straub *et al.*, 1993, 1994; Haining *et al.*, 1999), and *CYP3A* (Szklarz and Halpert, 1997; Roussel *et al.*, 2000; Domanski and Halpert, 2001) subfamilies as important for substrate turnover, within SRS4 of the *CYP2D* subfamily as important for electrostatic interactions with substrates (Ellis *et al.*, 1995; Modi *et al.*, 1996), and within SRS4 of the *CYP3A4* protein as important for substrate metabolism (Domanski *et al.*, 1998), have highlighted several critical SRS regions. Additional mutagenesis within SRS2, SRS5 and SRS6 regions of the *CYP2B1* protein (Kedzie *et al.*, 1991; He *et al.*, 1992, 1994; Halpert and He, 1993; Luo *et al.*, 1994; Szklarz *et al.*, 1995) and the *CYP3A4* protein (Harlow and Halpert, 1997; He *et al.*, 1997; Wang *et al.*, 1998) have identified other SRS regions important for substrate turnover. Additional mutagenesis outside known SRS regions in the *CYP2B5* protein (He *et al.*, 1998) has identified amino acids affecting catalytic activity in unexpected regions. To place the *CYP6B1* catalytic site within these contexts, we have developed a second stage model for the *P.polyxenes* *CYP6B1* protein docked with various substrates (xanthotoxin and bergapten) and inhibitors (coumarin and pilocarpine). Analyses of substrate-docked and substrate-free models have highlighted an unusual aromatic amino acid network present in the catalytic site of this insect P450 that facilitates positioning of linear furanocoumarins in the *CYP6B1* catalytic site.

Materials and methods

Chemicals

Xanthotoxin (8-methoxypsoralen), bergapten (5-methoxypsoralen), trioxsalen (4,5',8-trimethylpsoralen), psoralen, NADPH-regenerating components, other chemical reagents, heat-inactivated fetal bovine serum (FBS) and hemin were obtained from Sigma (St Louis, MO). Molecular biology reagents were supplied by GibcoBRL/Life Technology (Grand Island, NY). Isopimpinellin was obtained from Indofine Chemical Co. (Belle Mead, NJ). Sf9 insect cells, SF-900 serum-free medium, pFastBac1 expression vector and DH10BAC competent cells were purchased from GibcoBRL/Life Technology. Penicillin/streptomycin was obtained from Bio-Whittaker (Walkersville, MD).

Homology modeling, molecular dynamics and docking calculations

A multiple sequence alignment between the *CYP6B1* protein (Cohen *et al.*, 1992) and the *Bacillus megaterium* *CYP102* (Ruettinger *et al.*, 1989) and *P.glaucus* *CYP6B4* (Hung *et al.*, 1997) proteins was generated using the programs MOE (Chemical Computing Group, Inc.: <http://www.chemcomp.com/>) and ClustalW (<http://www.ebi.ac.uk/clustalw/>). The identical sequence alignments derived from this were subsequently homology modeled from PDB structures (Berman *et al.*, 2000) using the MOE program generating 10 models, with the explicit inclusion of the heme coordinates in all steps of the homology model generation. These models were subject to a coarse energy minimization procedure in order to remove possible van der Waals clashes between atoms. The best model with a score of -2.89889 using MOE's residue packing quality function was selected. Heme coordinates were duplicated from the *CYP102* crystal structure, and a covalent bond was created between the heme's iron atom and the sulfur of Cys443.

Molecular dynamics (MD) calculations on the apo form of the enzyme were run using the MOE program and the CHARMM22 (MacKerell *et al.*, 1998) force field as distributed in MOE and corrected to accurately represent all heme carbon atoms' hybridization (Chemical Computing Group, personal communication). In one MD simulation, no explicit water molecules were added to the homology model and a distance-dependant dielectric was used. The total simulation time in this case was 255.3 ps. In a second MD simulation, explicit water molecules were added to the homology model, using the 'soaking' facility in the MOE program and up to three hydration layers. The total simulation time in this case was for 170 ps. In both the fully hydrated and implicitly hydrated simulations, the canonical ensemble (NVT) was used with a target temperature of 300 K. An integration time step of 1 fs was used and structures were saved to disk every 100 steps. The entire system (protein + heme) was included with no atoms restrained or held fixed during the simulations. As in the case of energy minimizations, a distance-dependant dielectric and a non-bonded cut-off value of 7 Å were used.

Substrates were docked within the catalytic site using the Monte Carlo docking procedure of MOE after attaching a single oxygen to the heme plane (representing the iron-oxo intermediate). Parameters for the Fe–O bond and N–Fe–O bond angles were obtained using MOE's parameter assignment facility and are listed in Table I. Charges on the iron-oxo intermediate Fe and O atoms are calculated by MOE to be (0.642) and (–0.403) e.u., respectively. These charges and parameters, which are not based on *ab initio* parametrization of the force field, are attributed by MOE to be consistent with the rest of the CHARMM22 parameters. The structure and location of the two most widely distributed substrates of *CYP6B1*, xanthotoxin and bergapten, were initially placed above the heme plane, and allowed to vary through Monte Carlo

Table I. CHARMM22 force field parameters in the MOE program for heme Fe–O bond

	Fe–O bond	N–Fe–O angle
Atom types	FE-OH1	NHP-FE-OH1
Force constant	273.472 kcal/mol/Å ²	58.773 kcal/mol/degree ²
Equilibrium value	1.786 Å	90.0°

simulations removing bias due to manual placement. Twenty-five possible conformations were generated for each substrate inside the protein, and ranked according to the sum of the ligand's internal energy, van der Waals and electrostatic energy terms of the potential energy function, while keeping the side chains rigid. For xanthotoxin, the three best ranking and similar binding modes position the epoxidation site on the furan ring in closest proximity to the iron-oxo complex. For bergapten, the two best ranking but different binding modes have similar energies. The first of these modes has a similar orientation to that of xanthotoxin, and the second of these modes orients the substrate farther away from the heme. The first binding mode has the lowest van der Waals term and is compatible with an orientation allowing epoxidation to take place. The two best-ranked binding modes for xanthotoxin and bergapten were selected, included in the protein and the protein–substrate–heme complexes and energy minimized using the MMFF94s force field in MOE assuring that the final energy gradient was <0.01 kcal/mol/Å. In the protein–ligand minimizations, all protein side chains were fully flexible, while the heme coordinates were kept fixed to avoid any distortion of the heme plane due to the lack of bonded parameters for the heme in the MMFF94s force field. Interaction energies between the minimized protein and the ligand were calculated as the difference between the total potential energy of the minimized complex, and the sum of the individual protein and ligand components of the complex. The van der Waals and electrostatic contributions to this interaction energy were recorded and reported. Known inhibitors of CYP6B1, coumarin and pilocarpine, were docked using similar procedures without bias for their positioning relative to the heme iron.

The xanthotoxin and bergapten substrates were subjected to a second round of energy minimization imposing the substrate carbon to heme oxygen (C–O) distance to be 3.5 Å by setting a distance restraint on the C–O distance in the form of a penalty of 50 kcal/mol/Å. Substrates were positioned at 3.5 Å or closer by turning off this penalty. This 'pulling' has the effect of allowing the substrate to position itself closer to the heme by allowing it to cross potential energy barriers that might not be crossed in the standard energy minimization of the original unbiased docking mode. 'Pulling' energy minimizations were run until an energy gradient <0.01 kcal/mol/Å was achieved. The interaction energies between the protein and the substrate were calculated as described above and their van der Waals and electrostatic contributions calculated and reported for analysis.

Structures of the F484Y and F116Y mutants complexed with ligand were obtained by replacing individual amino acids within the MOE program, placing the ligand in the same initial orientation as in the wild-type species and energy minimizing the complex to an energy gradient of <0.01 kcal/mol/Å. The same 'pulling' energy minimization steps performed for the wild-type protein were run for each of the mutated species.

Baculovirus expression of CYP6B1 protein

CYP6B1 wild-type (6B1wt) coding sequences were subcloned from the original pVL1393 baculovirus vector (Ma *et al.*, 1994) into the pFastBac1 expression vector (GibcoBRL-Life Technology) using common BamHI and XbaI sites present in each sequence. Protocols for construction and expression of recombinant baculovirus using the Bac-to-Bac baculovirus expression system were as described by the manufacturer (GibcoBRL/Life Technology). Control viral stocks were

generated using pFastBac1 vector containing no foreign DNA. Recombinant wild-type CYP6B1 protein was expressed in Sf9 insect cells in SF-900 serum-free medium supplemented with 8–10% FBS, 50 µg/ml streptomycin sulfate and 50 U/ml penicillin. Sf9 cell cultures at a density of 0.8×10^6 cells/ml were infected at a multiplicity of infection (MOI) of 2 and supplemented with 5 µg/ml hemin at the time of infection. Insect cells expressing these constructs were harvested 72 h post-infection (PI) by centrifugation at 500 g for 5 min, resuspended in ice-cold cell lysate buffer [100 mM potassium phosphate (pH 7.8), 1.1 mM EDTA, 0.1 mM dithiothreitol and 0.5 mM phenylmethylsulfonyl fluoride, 5 µg/ml (w/v) leupeptin, 20% glycerol], lysed by sonication for 1 min and stored on wet ice during analysis. Packed cells collected from a 10 ml cell culture obtained from a single 100 mm² culture plate were resuspended in 1.0 ml of cell lysate buffer. Protein concentrations were determined using the Bradford (Bradford, 1976) method and the P450 concentration was measured by the method of Omura and Sato (Omura and Sato, 1964) using an extinction coefficient of 91 mM⁻¹ cm⁻¹ at 450 nm for the reduced CO complex.

P450 inhibition assays

Xanthotoxin and bergapten metabolism assays were run with 5 µM xanthotoxin or bergapten in a 0.450 ml reaction containing 100 µl of P450-expressing cell lysate, 0.5 U of glucose-6-phosphate dehydrogenase and 100 mM potassium phosphate buffer (pH 7.8). For control assays (lacking inhibitors), reactions were preincubated for 5 min at 30°C, and initiated by the addition of 50 µl of a NADPH-generating system (3 mM NADP, 30 mM glucose-6-phosphate, 10 mM MgCl₂) yielding a final reaction volume of 0.5 ml. After incubation at 30°C for 30 min in a shaking water bath, the reaction was terminated by the addition of 100 µl of ice-cold 2 N HCl, and 50–80 µl of another 5 µM furanocoumarin stock were added as an internal standard. The substrate remaining in each reaction was extracted by adding 0.5 ml of ethyl acetate, vortexing samples for 1 min, centrifuging them at 2000 g for 10 min and collecting the organic phase for direct analysis on a normal phase HPLC column as described in Cohen *et al.* (Cohen *et al.*, 1989). The furanocoumarin metabolism in each reaction was expressed as the percentage of the total furanocoumarin recovered in a control reaction acidified at time zero. The intra-day ($n = 6$) and inter-day ($n = 3$) accuracy of quality control (QC) samples for 1 and 5 µM xanthotoxin was acceptable at both concentrations with $<9\%$ deviation of the nominal values. The intra-day and inter-day relative standard deviation (CV) of the concentration of the QC samples was $<14\%$ at both concentrations. The enzyme activity calculated for wild-type CYP6B1 protein was expressed as picomoles of substrate metabolized per minute per nanomoles of P450 detected by CO difference analysis (Omura and Sato, 1964). In preliminary experiments, it was ascertained that during a 30 min incubation, the disappearance of xanthotoxin was linear from 50 to 500 µg protein/ml incubation mixture; during a 45 min incubation, the disappearance of xanthotoxin was linear up to a protein content of 500 µg/ml. For inhibitor assays, reaction mixtures were preincubated for 20 min with varying concentrations of each inhibitor [bergapten at 0.1–100 µM, xanthotoxin at 0.1–100 µM, coumarin at 1–3000 µM, pilocarpine at 1–3000 µM, ketoconazole at 0.1–100 µM, imidazole at 1–3000 µM, cimetidine at 1–3000 µM and cypermethrin at 1–1000 µM in the presence of NADPH and reactions were initiated by the

addition of 5 μM xanthotoxin (for most inhibitors tested) or by the addition of 5 μM bergapten (for xanthotoxin inhibition)]. Metabolism assays were conducted for 30 min and analyzed as above. The experiments were performed with cell extracts expressing wild-type CYP6B1 protein ($n = 4$).

Results

Homology modeling

The *P.polyxenes* CYP6B1 protein was homology modeled based on multiple sequence and structure alignments with the *B.megaterium* CYP102 (Ruettinger *et al.*, 1989) and the *P.glaucus* CYP6B4 (Hung *et al.*, 1997) proteins. The CYP102 protein represents the only soluble bacterial P450 with a defined crystal structure (Ravichandran *et al.*, 1993; Li and Poulos, 1994, 1997) that is capable of interacting with NADPH cytochrome P450 reductase during its catalytic cycle. It is also capable of metabolizing the linear furanocoumarin xanthotoxin but at an efficiency [$19.20 \text{ fmol min}^{-1}$ (pmol P450^{-1})] significantly lower than the CYP6B1 protein (Chen *et al.*, 2002). The CYP6B4 protein represents another insect P450 that metabolizes xanthotoxin and bergapten at efficiencies [3214 and $3541 \text{ pmol min}^{-1}$ (nmol P450^{-1}), respectively] higher than for the CYP6B1 protein (Hung *et al.*, 1997; Li *et al.*, 2003). Multiple sequence alignments of these three proteins generated using the programs MOE and ClustalW indicate that the CYP6B1 protein shares 64% sequence identity with CYP6B4 and 20.1% identity with the CYP102 protein. Similar sequence alignments with the rabbit CYP2C5 protein (Pendurthi *et al.*, 1990), which represents the only membrane-bound eukaryotic P450 with a defined crystal structure (Williams *et al.*, 2000), indicate that it shares a low similarity identity (20.9%) with the CYP6B1 protein. The CYP102 protein was chosen as the template for modeling the CYP6B1 structure rather than the CYP2C5 protein, since CYP102 and CYP6B1 are functionally related in their ability to metabolize xanthotoxin while CYP2C5 cannot metabolize this compound. In addition, our analysis of the CYP2C5 crystal structure (Rupasinghe *et al.*, 2003) has indicated that it has low Prosa II normalized Z-scores and low Profile 3D-1D self-compatibility scores, raising the possibility that it has several misfolded regions incorporated into its structure. Additional studies have also indicated that incorporation of the CYP2C5 structural coordinates into models of other P450s strongly bias the models' binding site structures (Kirton *et al.*, 2002). For these reasons and because the sequence identities between CYP102 and CYP6B1 versus CYP2C5 and CYP6B1 are very similar, we chose to use the CYP102 protein for our structural template to minimize the inclusion of potentially misfolded regions into the CYP6B1 structure.

Due to a high level of amino acid variation, significant variations occur in the primary sequence alignments of the SRS1 region (between helices B and C) of the CYP6B1, CYP102 and CYP2C5 proteins (Figure 1). Primary sequence alignments for representative members of the CYP6B subfamily existing in *Papilio* and *Helicoverpa* exhibit significantly fewer variations with substitutions occurring only at residues 113 and 115 in the entire SRS1 region (Figure 1). Despite their high level of sequence heterogeneity, the secondary structures of the B and C helices bounding this region are well conserved among the CYP6B1, CYP102 and CYP2C5 proteins. Between these two helices, the predicted helices and loop structures vary more with the CYP6B1 protein predicted to contain an 11

SRS1	B'-helix	B'-C loop	C-helix
CYP102	SQALKEFVRDFA	GDGLFTSWTHE	KNWKAHNILLPSF 107
CYP2C5	GRGSVPILEKV	SRKGLGIAFSNA	KTWKEMRRFSLMTL 131
		113 115	
CYP6B1	DRGVEFSLDGL	GANIFHADG.D	R.WRSLRNRFTPLF 134
CYP6B3	DRGVEFSLDGL	GANIFHADG.D	R.WRSLRNRFTPLF 134
CYP6B4	DRGVEFSEEGE	GLNIFHADG.D	R.WRVLRQCFPTPLF 134
CYP6B17	DRGIEFSEEGE	GLNIFHADG.D	R.WRVLRQAFPTPLF 134
CYP6B6	DRGVEFSKEGL	GSNLFHADG.E	T.WRALRNRFTPIF 136
CYP6B7	DRGVEFSKEGL	GQNLFHADG.E	T.WRALRNRFTPIF 136
CYP6B8	DRGVEFSKEGL	GQNLFHADG.E	T.WRALRNRFTPIF 136
CYP6B9	DRGVEFSKEGL	GSNLFHADG.E	T.WRALRNRFTPIF 136
CYP6B10	DRGVEFSKEGL	GSNLFHADG.E	T.WRALRNRFTPIF 136
CYP6B27	DRGVEFSKEGL	GQNLFHADG.E	T.WRALRNRFTPIF 136
		SRS1	
		484	
SRS6			
CYP6B1	PSMKSSGPFKFDPMRLFALPKGGIYVN		
CYP6B3	PSNKSSGGEFKFDPMRLFVLPKGGIFVN		
CYP6B4	PSTKTMSEFSYDPTLLVYPKSGIFLN		
CYP6B17	PSTKTKSQFIYDPMRLFVYPKSGIFLN		
CYP6B6	PSKNTDRNLQVEPHRGLIGPKGGIRVN		
CYP6B7	PSKNTDRNLQVEPRRVTIIGPKGGIRVN		
CYP6B8	PSKNTDRNLQVEPRRVTIIGPKGGIRVN		
CYP6B27	PSKNTDRNLQVEPHRGLIGPKGGIRVN		
		SRS6	

Fig. 1. Sequence alignment between representative CYP6B subfamily members and the CYP102 and CYP2C5 templates in the SRS1 and SRS6 regions.

amino acid B' helix comparable with the 11 amino acid B' helix present in the CYP102 protein (Ravichandran *et al.*, 1993; Li and Poulos, 1994, 1997) that is lacking in the CYP2C5 protein (Williams *et al.*, 2000). As a result, variable sequences for this B-C region of the CYP6B1 protein are described as existing in its B' helix and B'-C loop and have been adjusted for the backbone coordinates present in the CYP102 protein (22 amino acids). For clarity, sequences for this region of the CYP2C5 protein are described as existing in its B-C loop because amino acid insertions/deletions approximate the same region as the B' helix and B'-C loop.

Homology modeling and energy minimization of the CYP6B1 apoprotein as described in Materials and methods generates a structure whose Ramachandran map shows 10 residues in 'generous' and five residues in 'outside' regions of the (ϕ , ψ) map (including Gly and Pro) out of a total of 498 residues. By this analysis, ~97% of the residues are in allowed and core regions indicating that our current model is of a similar quality to those published for bacterial CYP119 (Chang and Loew, 2000), CYP105C1 (Chang and Loew, 1996) and mammalian CYP2B4 (Chang *et al.*, 1997). Calculation of the normalized Prosa II score [Prosa II (version 3.02), Center for Applied Molecular Engineering, University of Salzburg, Austria] yields a global score of -0.65 , similar to that of other homology modeled P450 structures (Chang and Loew, 2000; Rupasinghe *et al.*, 2003). The Prosa II profile suggests that the α -domains regions comprising the residues in the 150–250 range are of a poorer structural quality (high Prosa II scores) than the other regions of the mode with negative scores (< -0.7) indicating correctly folded structures. None of the amino acids in the high Prosa II score region come in contact with the substrate in our docking predictions. As previously suggested for our first substrate-free CYP6B1 model derived using the program Quanta96/CHARMm/Modeler (Chen *et al.*, 2002), the side chains of Phe484, Phe116 and His117 are positioned in the catalytic site at nearly right angles to one

another above the heme plane. In our newer MOE-derived model (Figure 2a and b), the side chain of Phe371 is also projected into the catalytic site in a configuration that allows for a more extensive aromatic network consisting of Phe371, Phe484, Phe116, His117 and Tyr218. The presence of Tyr218 in this network results from the inclusion of a large flexible loop containing Leu214 to Leu222. This region is difficult to model with precision, as suggested by the relatively high Prosa II score of the two α -domains around this loop (between SRS2 and SRS3) that can be modeled in two different orientations. In one case, this loop orients Tyr218 towards the active site (in blue in Figure 2b), in the second case, the loop projects Tyr218 outside of the active site (in yellow in Figure 2b). The model that projects Tyr218 inside the CYP6B1 active site has a slightly better MOE score (-2.82) than the model that orients Tyr218 outside the active site (-2.85), and was selected for use in subsequent ligand–protein docking. The distances between the residues (i.e. between the center of the aromatic rings) in the active site in the apoprotein (Table II) and their orientation relative to one another are compatible with a stabilizing resonant network forming the catalytic pocket of the enzyme. As described by Burley and Petsko (Burley and Petsko, 1985) and Singh and Thornton (Singh and Thornton, 1985), such aromatic–aromatic interactions are typified by ring center distances between 4.5 and 7.0 Å and dihedral angles between 50 and 90°. This network highlights the key position of Phe484 in the CYP6B1 structure that is replaced by Leu484 and Leu437 in the insect CYP6B4 and bacterial CYP102 proteins (Figure 1). The side chains of Ile115 and Ala113 that are variable within the *CYP6B* subfamily are located on the side of the heme with distances of 3.4 and 9.8 Å, respectively, to the carbon of the heme's carbonyl group.

Substrate docking

Substrates were docked within the active site using the Monte Carlo docking procedure of MOE and repeated cycles of protein and substrate minimization. During the initial stage of the docking procedure, the side chains of the protein are fixed. The best-ranking docking modes of the ligands are identified and energy minimized in the protein, while allowing full side chain flexibility. The unbiased and lowest energy docking modes within 7.5 Å of the heme for xanthotoxin (Figure 3) and bergapten (Figure 4) in the CYP6B1 catalytic site are those having the furan ring oriented towards the iron-oxo (or iron-hydroperoxy) intermediate formed during the catalytic cycle. Figure 3 illustrates the amplitude of the structural changes of the substrate–protein complex upon energy minimization. This positioning indicates that the closest substrate atom to the heme is the 2' carbon that would be attacked in an epoxidation reaction, with a distance of 3.5 Å for both xanthotoxin and bergapten. Each of these substrates has its methoxy group pointing in a different orientation: towards Phe116 in the case of bergapten (Figure 4) and away from Phe116 in the case of xanthotoxin (Figure 3). Residues Asp101, Phe371, Phe484, Ala485, Thr307, Asp370, Ala369, Val104, Thr372, Gln373, Phe116 and Ala303 are predicted to contact the substrate with the contact map calculated by the MOE program shown in Figure 5. In this, the meshed regions in green (for hydrophobic contacts) and red (for hydrogen bonding capacities) correspond to possible regions where preferred interactions with the protein are predicted to occur. Interestingly, this preferred contacts map almost exactly overlays the location of the substrate (xanthotoxin in Figure 5). Around a large central

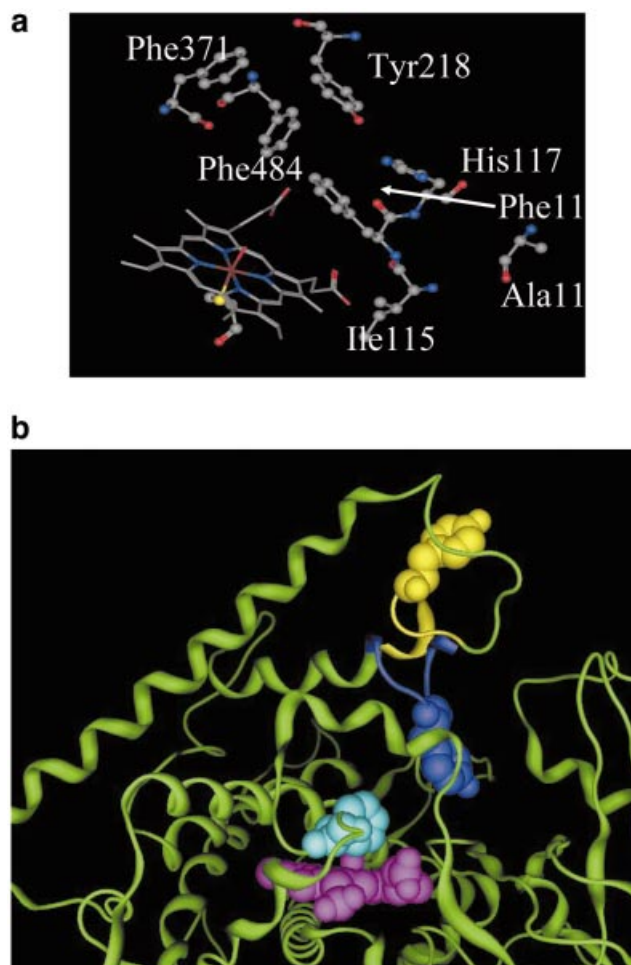


Fig. 2. Detail of the active site in CYP6B1 apoprotein. (a) The catalytic site of CYP6B1 derived from structure modeling with CYP102 as the template is shown with amino acids participating in the aromatic network above the heme plane. (b) The two possible orientations of the Leu214 to Leu222 loop in the CYP6B1 model are shown with the heme in purple, the backbone and Tyr218 atoms projecting outside the active site in yellow and the backbone and Tyr218 atoms projecting towards the active site in blue.

Table II. Distances (Å) between residues in the CYP6B1 apoprotein

	F484/F116	F484/Y218	F371/F484	F116/H117	F484/H117
Distance	5.4	4.4	6.4	4.3	7.3

hydrophobic region, corresponding to the resonant core of the substrate, are located four possible hydrophilic regions, labeled A–D. Region A corresponds to the location of the 8-methoxy group on xanthotoxin. Region B, symmetrical to region A, corresponds to the location of the 5-methoxy group on bergapten. Region C accommodates the two oxygen atoms on the lactone ring (opposite the furan ring). Region D could accommodate a hydrogen-bond donor capable of interacting with the iron-oxo intermediate. The location of region C explains why the lactone ring's oxygen atoms are oriented the same way in both xanthotoxin and bergapten; the existence of regions A and B explains why both the 8-methoxy

(xanthotoxin) and 5-methoxy (bergapten) orientations are allowed as well as the bifunctional 8-methoxy, 5-methoxy (isopimpinellin). Binding of these furanocoumarins signifi-

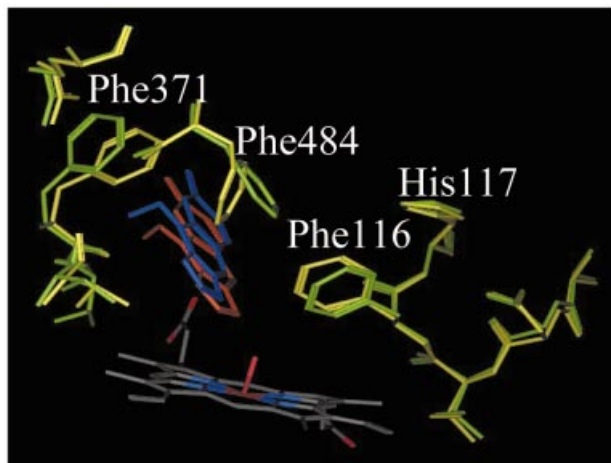


Fig. 3. Structure of the CYP6B1–xanthotoxin complex. The structure of the CYP6B1 protein in the CYP6B1–xanthotoxin complex is shown before energy minimization (yellow) and after energy minimization (green) of the complex. The position of the substrate in the CYP6B1–xanthotoxin complex is shown before energy minimization (blue) and after energy minimization (red). Hydrogen atoms have been omitted for clarity.

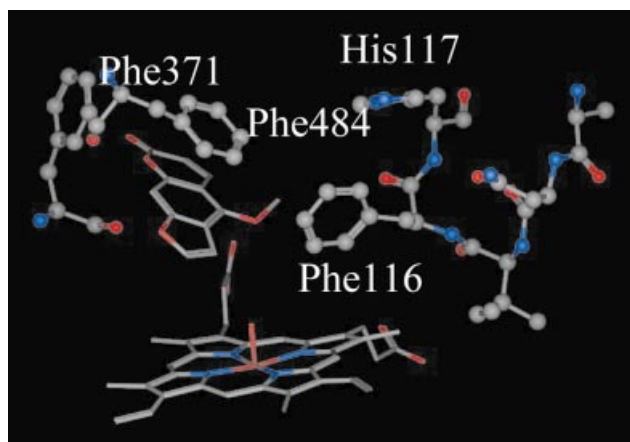


Fig. 4. Structure of the energy minimized CYP6B1–bergapten complex.

cantly changes the relative orientation of the phenyl rings of Phe484 and Phe116 (Figures 3 and 4) such that the phenyl ring of Phe484 is parallel to the central resonant ring of both xanthotoxin and bergapten, allowing for a π -stacking conformation that would stabilize protein–substrate interactions as we had previously predicted from our Phe484 replacements (Chen *et al.*, 2002). In this reoriented position, the distance between Phe484 and Phe116 is not dramatically affected but the resonant aromatic network formed with these residues is disrupted.

For both substrates, an additional round of energy minimization was performed, imposing a restraint on the distance of 3.5 Å between the heme oxygen and the substrate carbon attacked in this reaction, as described in Materials and methods. The final interaction energy computed in the case of the energy minimized protein–substrate complex with this closer substrate oxygen distance is given in Table III, together with the van der Waals and electrostatic contributions to the interaction energies. The potential interaction energies between the substrates and the enzyme are calculated to be –42.5 kcal/mol for xanthotoxin and –52.0 kcal/mol for bergapten. The 9.5 kcal/mol difference in the interaction energy in the case of bergapten and xanthotoxin originates mainly in a more negative van der Waals contribution, suggesting the existence of more steric repulsions in the binding of xanthotoxin that are not fully removed upon the energy minimizations performed here. When pulled 0.5 Å closer to the heme while energy minimizing the structure, the substrate–protein interaction energies are calculated to be more stabilizing by up to 5.8 kcal/mol (Table III). These values suggest that the enthalpic (potential) energy contribution to the binding free energy of bergapten would be slightly more stable than for xanthotoxin, and that movement of the substrates to reaction positions closer to the heme would be favored by the protein environment.

Table IV presents substrate–residue interaction energies between xanthotoxin or bergapten and P450 residues that have at least one atom within 5.0 Å of the substrate, which account for ~80% of the total substrate–enzyme interactions. Values in this table were calculated in the case of the ‘pulled’ energy minimized structures. Comparison of the substrate–residue interaction energies for each of the two substrates indicates differences in interaction with some residues that would not be obvious from a purely structural consideration. For instance, bergapten appears to interact with the heme moiety twice as strongly as xanthotoxin, and bergapten interactions with residues Asp101, Val104, Ala303, Asp370 and Thr372 are also significantly more stable than interactions

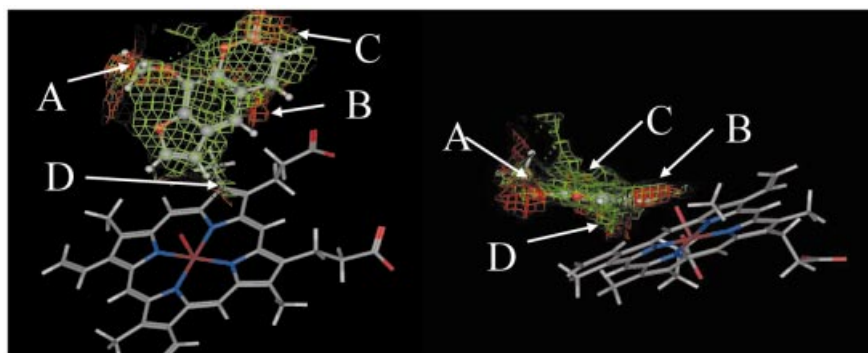


Fig. 5. CYP6B1–ligand contact maps. The xanthotoxin contact maps are shown with the hydrophobic contact regions shown in green and the hydrophilic contact regions shown in red.

with xanthotoxin. Conversely, xanthotoxin interactions are more stable with residues Phe371 and Gln373. In other cases, substrate–residue interactions are repulsive: Phe116 with both substrates (more repulsive for xanthotoxin), Thr370 (more repulsive for bergapten) or Thr307 (xanthotoxin only). However, other residues do not exhibit any marked differences in the amplitude of interactions with one or another of the

Table III. Ligand–enzyme interaction energies with their van der Waals and electrostatic contributions (kcal/mol)

		(a)	(b)	Electrostatic	van der Waals
Wild-type	Bergapten	-52.0	-53.6	-41.3	-12.3
	Xanthotoxin	-42.5	-45.0	-43.4	-1.6
	Coumarin	-38.0			
	Pilocarpine	-46.8	-50.0		
F116Y	Bergapten	-48.1	-59.2	-46.6	-12.6
	Xanthotoxin	-48.2	-50.8	-44.0	-6.8
F484Y	Bergapten	-48.5	-31.4	-26.7	-4.7
	Xanthotoxin	-50.0	-40.5	-30.6	-9.9

(a) Docked conformation. (b) After ‘pulling’ energy minimizations with a C–O distance of 3.5 Å.

substrates investigated here: Val368, Ala369, Phe484, Ala485, Leu486 and Ile299 (which actually has no substrate interactions). This table predicts residues that interact preferentially with one substrate, exemplifying the need for a concerted structural–energetic approach to ligand binding in proteins. It is interesting to note the suggested significant preference of the heme moiety for interactions with bergapten; however, the effect of iron-oxo oxygen’s charge on the interaction energy, such as might originate from an *ab initio* parametrization of the force field, has not been investigated here.

Molecular dynamics and model stability

To further define the stability of the energy minimized apoprotein and substrate-bound models, MD simulations were performed. Figure 6 shows the time series of thermodynamic and structural properties of the CYP6B1 apoprotein model computed both without and with explicit hydration (left versus right panels). In the top set of panels, the implicit-solvation MD converges at 300 K (± 10 K) within the first 50 ps of the simulation and the explicit-solvation MD converges to the target temperature within 100 ps. In the middle panels, the r.m.s.d. of each frame is compared with the initial frame after alignment to the backbone atoms. Importantly, for both the

Table IV. Interaction energies (kcal/mol) between P450 residues and substrates in the case of ‘pulled’ energy minimized structures

	Heme	F99	D101	V104	F116	I299	A303	T307	V368	A369	D370	F371	T372	Q373	F484	A485	L486
X	-9.9	-1.4	-1.7	-0.9	+2.2	0.0	+0.9	+1.0	-0.2	-3.6	+0.7	-5.6	-0.8	-8.8	-3.8	-3.1	-2.0
B	-17.9	-3.5	-6.7	-3.1	+1.0	0.0	-2.5	-0.8	-0.3	-2.9	+2.4	0.0	-3.0	-3.0	-2.2	-4.0	-1.0

X, xanthotoxin; B, bergapten.

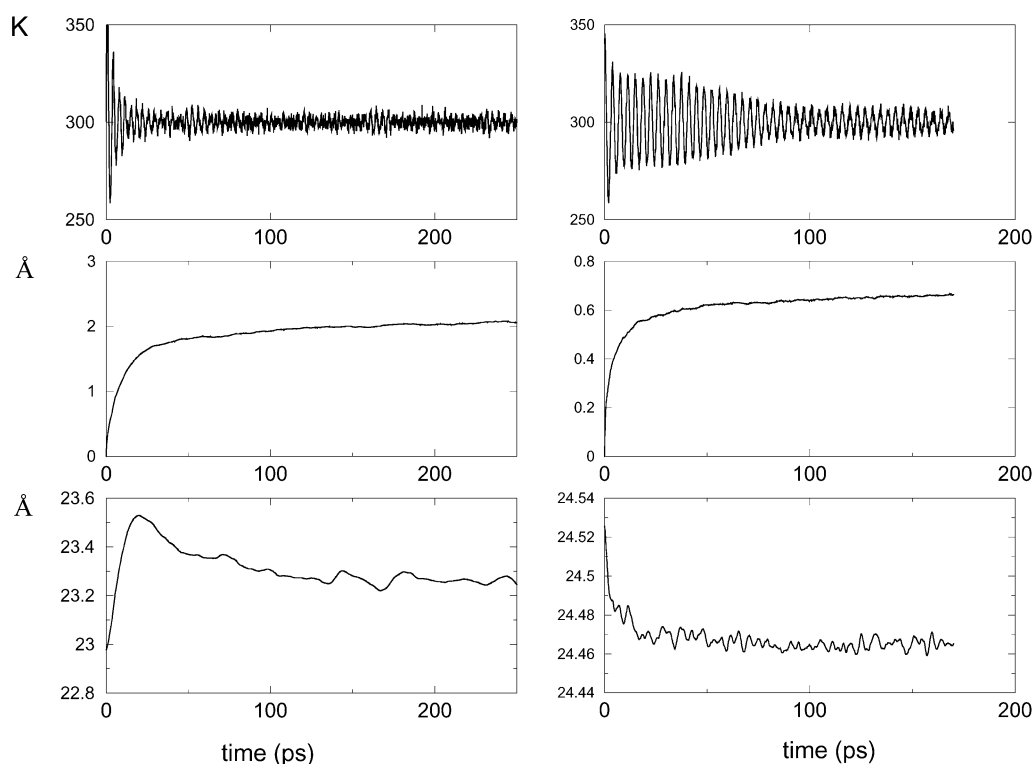


Fig. 6. Time series of thermodynamic and structural parameters during the MD runs. (Left) 250 ps run, no explicit hydration. (Right) 172 ps with explicit hydration. (Top) Temperature (K); (middle) r.m.s.d. compared with the initial frame (Å); (bottom) radius of gyration (Å).

implicit- and explicit-solvation MDs, these r.m.s.d.s plateau after ~50 ps. In the bottom panels, the radii of gyration of the protein during the course of the MD simulation plateaus in ~50 (implicit hydration) and ~25 ps (explicit hydration). These last results indicate quite strongly that the CYP6B1 apoprotein model used for subsequent docking calculations is thermodynamically stable and without major structural and/or folding rearrangements during the course of the MD simulation. In further support of this point, Figure 7 presents the superposition of active site residues for each of the two MD simulations, as well as for the energy minimized homology model used for docking calculations. It is apparent from these comparisons, that although some side chain rearrangements can occur during the MD simulations, the general structure of the active site is well preserved.

Inhibitor analysis and inhibitor docking

The range of compounds analyzed for inhibition of CYP6B1 metabolism of xanthotoxin was determined at 5 μM xanthotoxin and varying bergapten (0.1–100 μM), pilocarpine (1–3000 μM), coumarin (1–3000 μM), ketoconazole (0.1–100 μM), imidazole (1–3000 μM), cimetidine (1–3000 μM) and cypermethrin (1–1000 μM) concentrations (Figure 8). Based on our quantitations, the yields of functional P450 in CYP6B1 cell lysates ranged from 150 to 1000 pmol/10 ml plate culture and represented ~2–4% of the total cell protein at viral infection ratios (MOI) of 2. In these assays, bergapten inhibited CYP6B1-mediated metabolism of xanthotoxin with an IC_{50} value of 20 μM . In an additional experiment that is not shown, inhibition of CYP6B1 metabolism of bergapten was determined at 5 μM bergapten and varying xanthotoxin (0.1–100 μM). In this assay, xanthotoxin blocked CYP6B1-mediated metabolism of bergapten with an IC_{50} value of 8 μM . At low concentrations (0.3 μM) of either furanocoumarin, no difference in inhibition was observed between xanthotoxin and bergapten; at high concentrations (>3 μM), xanthotoxin was a

more effective inhibitor than bergapten. Among the other inhibitors, pilocarpine (a cholinomimetic natural alkaloid) inhibited xanthotoxin metabolism in a concentration-dependent fashion with an IC_{50} value of 22 μM . Imidazole and cimetidine inhibited xanthotoxin metabolism in a mechanism-based manner. Ketoconazole and coumarin had only marginal inhibitory effects with IC_{50} values over 70 and 1000 μM , respectively, and cypermethrin had no effect on this activity.

The inhibitory effects of buffer components on xanthotoxin metabolism were also analyzed at varying EDTA (0.1–30 μM) and NaCl (1–300 μM) concentrations. In these assays (Figure 8), up to 30 μM EDTA and up to 300 μM NaCl had no significant effect on the metabolism of xanthotoxin. At 300 μM or higher, NaCl inhibited the metabolism by 13% due to the partial protein denaturation as evidenced by the appearance of a minor absorbance at 420 nm. Similar analysis of the inhibitory effects of three organic solvents commonly used to prepare furanocoumarin substrates (methanol, acetonitrile, dimethyl sulfoxide) indicated that all of them inhibited xanthotoxin metabolism in a concentration-dependent manner with the rank order of DMSO > ACN > MeOH.

In conjunction with our analysis demonstrating that CYP6B1 cannot metabolize coumarin, the observed weak coumarin inhibition indicates that coumarin cannot be positioned in close enough proximity to the heme iron for catalysis and that it cannot displace xanthotoxin from the catalytic site. The lowest energy binding mode for coumarin, the weak CYP6B1 inhibitor, is shown in Figure 9. Importantly, the binding mode of coumarin does not disrupt the aromatic network predicted in the CYP6B1 apoprotein. On the contrary, coumarin seems to bind above the level of the Phe484–Phe116 interaction at a position too far from the heme to allow for substrate modification. Even so, the orientation of coumarin in the binding site is capable of competing with the binding of xanthotoxin and bergapten. The potential interaction energy between the inhibitor coumarin and the enzyme (Table III) is calculated to be –38 kcal/mol, substantially higher than for the

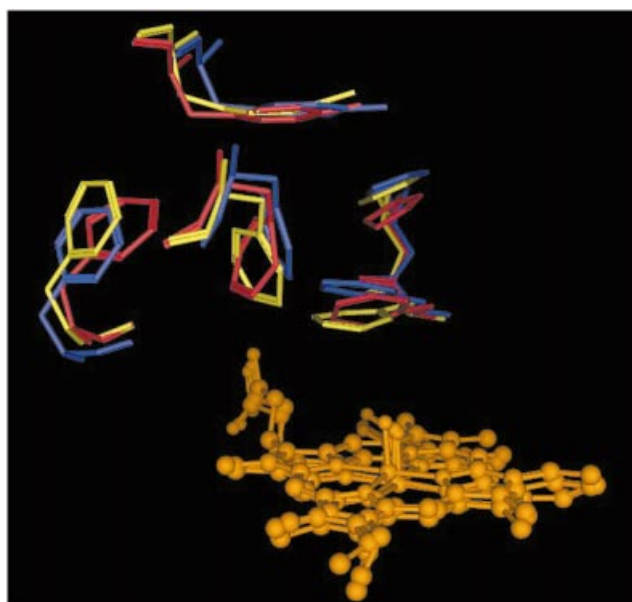


Fig. 7. Details of the active site in the CYP6B1 apoprotein after MD simulations. Superposition of active site residues in the last frame of the explicitly hydrated CYP6B1 model (red), implicitly hydrated CYP6B1 model (yellow) and minimized structure used for docking (blue). The heme atoms are shown in orange balls and sticks.

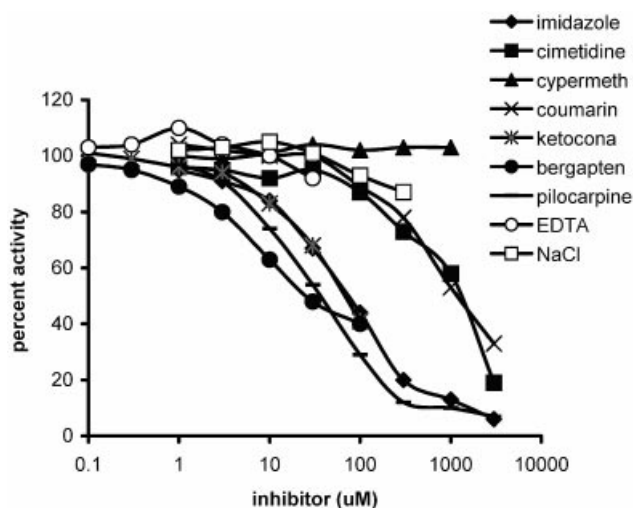


Fig. 8. Influence of various compounds on xanthotoxin metabolism by CYP6B1. *In vitro* reactions containing baculovirus-expressed CYP6B1 were preincubated for 20 min at 30°C in the presence of NADPH and varying inhibitor concentrations and subsequently incubated with 5 μM xanthotoxin for 30 min at 30°C. Activities were recorded as the percentage of activity remaining compared with control reactions lacking inhibitors incubated for the same periods of time.

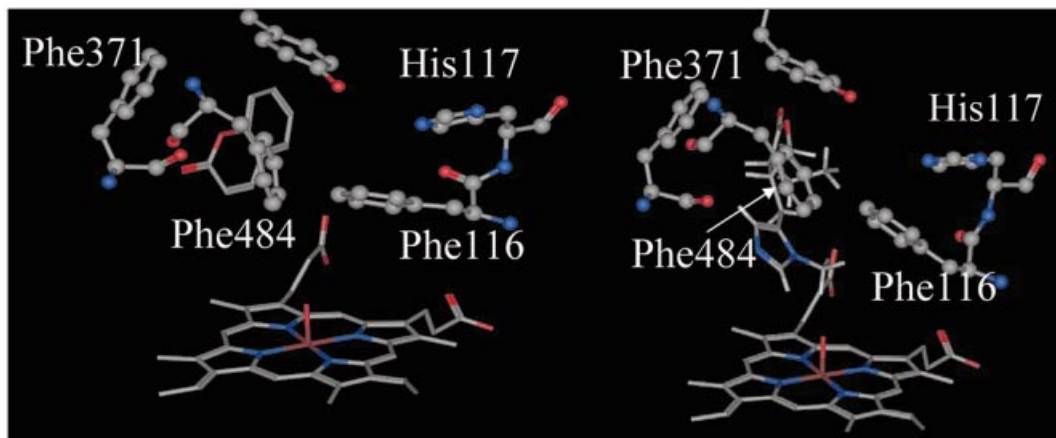


Fig. 9. Structures of the energy minimized CYP6B1–coumarin complex (left) and the energy minimized CYP6B1–pilocarpine complex (right).

substrates xanthotoxin and bergapten. Additional calculations, including MD simulations and free energy calculations, are required to confirm these values.

Molecular docking of the inhibitor pilocarpine in the active site of the CYP6B1 protein positions the imidazole nitrogen atom above the heme iron (Figure 9). The calculated interaction energy between the inhibitor pilocarpine and the enzyme (Table III) is calculated to be -46.8 kcal/mol and is very similar to that calculated for the substrate xanthotoxin. The existence of potential interactions between the imidazole ring of pilocarpine and the heme moiety suggests the possibility that pilocarpine coordinates to the heme via a nitrogen–iron interaction.

Effects on docking of amino acid replacements in SRS1

Docking of the substrates in the F116Y and F484Y mutants was investigated as described in Materials and methods. As shown in Table III, the F484Y mutant exhibits a stronger interaction with the substrate xanthotoxin and a weaker interaction with the substrate bergapten at ligand–heme distances of ~ 4 Å, when compared with that of the wild-type. At shorter distances of 3.5 Å, which would correspond to closer approaches of the substrate and heme, the interaction energies increase by 9.5 kcal/mol in the case of xanthotoxin and by 17.1 kcal/mol in the case of bergapten. This indicates that the F484 mutant can accommodate these substrates at 4 Å from the heme with approximately the same energy as for the wild-type protein but not at shorter reaction distances. In contrast to this, the F116Y mutant stabilizes both substrates closer to the heme as in the case of the wild-type protein. As shown in Table III, the balance between the van der Waals and electrostatic contributions to the ligand–enzyme interaction energies for the F116Y and F484Y mutants shows significantly different effects. In the case of the binding of bergapten, the F116Y mutation makes the electrostatic contribution more negative than in the wild-type protein, while the van der Waals contribution is not significantly modified. In the case of the binding of xanthotoxin, the F116Y mutation makes the van der Waals contribution more negative, while the electrostatic contribution sees a very small change. In the case of the binding of bergapten, the F484Y mutation makes both the electrostatic and van der Waals contributions more positive while, in the case of the binding of xanthotoxin, the F484Y mutation makes the electrostatic contribution more positive

and the van der Waals contribution more negative than for the wild-type protein.

Discussion

This homology modeling has provided substantial information on the identity of amino acids in the *P. polyxenes* CYP6B1 catalytic site moderating furanocoumarin metabolisms. Modeling of this protein against the crystal structures of the bacterial CYP102 protein and comparison with the insect CYP6B4 protein, another furanocoumarin-metabolizing P450 and the vertebrate CYP2C5 protein has indicated that despite the substantial divergences in primary sequences for these proteins (CYP6B1 and CYP102 are 20.1% identical; CYP6B1 and CYP2C5 are 20.9% identical), their secondary and tertiary structures are as highly conserved as in other bacterial and mammalian P450s (Graham-Lorence and Peterson, 1996; Dai *et al.*, 2000; Williams *et al.*, 2000). Alignments of the CYP6B1 protein sequence against these others indicate that its SRS1 region is extended to include a structured B' helix identical in length to that in the bacterial CYP102 protein (Ravichandran *et al.*, 1993; Li and Poulos, 1994, 1997) and a more extended B'-C loop in contrast to the less structured B-C loop in the vertebrate CYP2C5 protein (Williams *et al.*, 2000). Structural overlays of our predicted CYP6B1 apoprotein structure with the region between the B-C helices in the CYP2C5 and CYP102 crystal structures indicate an r.m.s.d. of C α atoms of < 1 Å for four amino acids at the middle of the B'-C loop (including Phe116 and His117) and an r.m.s.d. of C α atoms of < 2 Å for the remaining C-terminal region of the B-C loop. These relatively small variations in the structure of the B-C region are significant given this region's high degree of sequence variability in other P450s (Gotoh, 1992; Chang and Loew, 2000) and its role in defining substrate specificity (von Wachenfeldt and Johnson, 1995; Chang and Loew, 2000; Domanski and Halpert, 2001).

Coupled with our previous study on the role of the invariant Phe116 and His117 in CYP6B1 (Chen *et al.*, 2002), our furanocoumarin-docked model indicates quite conclusively that, within this prototypical member of the *CYP6B* subfamily, amino acids within the SRS1 region contribute significantly to defining the configuration of the catalytic site as well as the range of furanocoumarins metabolized. As predicted from substrate docking, the side chain of Phe484 in the SRS6 region

is located at distances of 3.9 and 4.6 Å from the oxidation site on the furan ring of xanthotoxin and bergapten, respectively. This model, which implies that Phe484 has a dual role in the maintaining the aromatic network of the catalytic site and positioning of furanocoumarins in the catalytic site, has been supported by many mutations. Specifically, all Phe484 replacements to other aromatic amino acids maintain the configuration of the catalytic site as monitored by the ability to generate CO difference maxima at 450 nm while disrupting its ability to metabolize furanocoumarins.

Our furanocoumarin-docked model also indicates that the side chain of Thr307 in the SRS4 region is located in close proximity to the reactive oxygen at distances of 3.4 and 3.7 Å in the xanthotoxin-docked and bergapten-docked models, respectively. This side chain that is preceded by an acidic residue (Glu306) corresponds to Thr252 in the bacterial CYP101 protein that is preceded by an acidic residue (Asp251). Site-directed mutagenesis in this bacterial P450 has indicated that these side chains are essential for dioxygen activation through a distal pocket charge relay mechanism (Martinis *et al.*, 1989; Gerber and Sligar, 1992, 1994). The spatial positioning of these residues in our CYP6B1 model is similar enough to suggest that these side chains participate in dioxygen activation.

Analyzing the interactions of different inhibitors in the P450 active site affords another approach to probing active site structures in the P450 proteins. In several cases, vertebrate P450s are known to be non-competitively and competitively inhibited by linear furanocoumarins. Specifically, xanthotoxin competitively inhibits coumarin 7-hydroxylation in human microsomes and multiple furanocoumarins, including xanthotoxin, inhibit coumarin 7-hydroxylation in mouse microsomes (Maenpaa *et al.*, 1993a,b, 1994). Analysis of specific vertebrate isozymes indicates that xanthotoxin, bergapten and psoralen all have the ability to suicide-inactivate human CYP2A6 protein (Koenigs *et al.*, 1997; Koenigs and Trager, 1998; Kharasch *et al.*, 2000). Bergapten suicide-inactivates human CYP3A4 (Ho *et al.*, 2001) and xanthotoxin competitively inhibits a variety of drug metabolisms by CYP3A4 (Lown *et al.*, 1997). The strong contrast of these results with the high rates of xanthotoxin metabolism observed for the insect CYP6B1 protein as well as its ability to be inhibited by coumarin indicate that the geometries of these vertebrate and insect active sites have evolved independently. Comparison of the previously published CYP2A6 model (Lewis *et al.*, 1999) with our CYP6B1 model (data not shown) identifies very different binding modes for xanthotoxin and coumarin in these catalytic sites and specific residues (Phe484 in CYP6B1), which stabilize interactions with the larger three-ring furanocoumarins and prevent coumarin from effectively binding near the catalytic core of this P450.

In addition, pilocarpine, a cholinomimetic natural alkaloid, competitively inhibits the coumarin 7-hydroxylase activity of CYP2A6 with an IC₅₀ value of 1.21 μM (Kinonen *et al.*, 1995). It has been assumed that the mechanism of CYP2A6 inhibition by pilocarpine involves heme ligation via the imidazole ring nitrogen atom (Lewis *et al.*, 1999). Our data indicate that pilocarpine inhibits CYP6B1 at a similar IC₅₀ (22 μM) and also suggests the possibility that pilocarpine inhibits the CYP6B1 protein by heme ligation.

The results of the docking calculations show that the energetic implications of mutation of the two Phe residues, F484 and F116, in the active site have opposite effects on

substrate binding. While the F116Y mutation is not predicted to destabilize substrate–enzyme interactions at an optimal reaction distance from the heme, the F484Y mutant is predicted to destabilize protein–substrate interactions at reduced reaction distances. Again, it must be remembered that the present calculations deal with potential energies only and that entropic effects that contribute to the total binding free energy are not taken into account in these calculations. Within this approximation, the present results are in agreement with the experimental observations that the F116Y mutation maintains half of its enzymatic activity towards bergapten and little activity towards xanthotoxin, while the F484 mutation suppresses all enzymatic activity (Chen *et al.*, 2002).

Homology modeling techniques are not exempt from a certain level of serendipity that requires the use of analytic methods to investigate the quality of the model. Ultimately, however, a model must be able to generate hypotheses that can be compared with experiments. It was the goal of the present paper to obtain a model that could be evaluated with respect to experimentally tested mutants and provide a further rationale for the effects of individual mutants. Not unlike homology models of other proteins, our CYP6B1 model predicts several possible orientations for the Tyr218 residue but the use of the most energetically favored of these structures generates a Ramachandran map indicative of a structurally sound model. In addition to this static structural analysis, MD simulations have shown that the model is energetically stable over relatively long simulation times. Calculations of substrate–enzyme potential interaction energies derived from this model agree qualitatively with the experimental observations and provide for qualitative interpretations of enzyme activities in terms of binding energy between the substrate and the enzyme. Together, these data contribute significantly to our understanding of the efficient metabolism of various furanocoumarins by this insect P450 and, in the long term, can provide insight into the P450-based mechanisms modulating furanocoumarin-mediated drug sensitivities in humans.

Acknowledgements

We thank Mr Sanjeeva Rupasinghe for useful discussions on the homology models and Dr Stephen Sligar for critical comments on the manuscript. This work was supported by National Institute of Health grant RO1-GM50007.

References

- Ameer,B. and Weintraub,R.A. (1997) *Clin. Pharmacokinet.*, **33**, 103–121.
- Anderson,T.F. and Voorhees,J.J. (1980) *Annu. Rev. Pharmacol. Toxicol.*, **20**, 235–257.
- Apseloff,G., Shepard,D.R., Chambers,M.A., Nawoot,S., Mays,D.C. and Gerber,N. (1990) *Drug Metab. Dispos.*, **18**, 298–303.
- Berenbaum,M.R. (1991) In Rosenthal,G. and Berenbaum,M.R. (eds), *Herbivores: Their Interactions with Secondary Plant Metabolites*. Academic Press, San Diego, pp. 221–249.
- Berenbaum,M.R., Favret,C. and Schuler,M.A. (1996) *Am. Nat.*, **148**, S139–S155.
- Berman,H.M., Westbrook,J., Feng,Z., Gilliland,G., Bhat,T.N., Weissig,H., Shindyalov,I.N. and Bourne,P.E. (2000) *Nucleic Acids Res.*, **28**, 235–242.
- Bradford,M.M. (1976) *Anal. Biochem.*, **72**, 248–252.
- Burley,S.K. and Petsko,G.A. (1985) *Science*, **229**, 23–28.
- Chang,Y.T. and Loew,G.H. (1996) *Protein Eng.*, **9**, 755–766.
- Chang,Y.T. and Loew,G.H. (2000) *Biochemistry*, **39**, 2484–2498.
- Chang,Y.T., Stiffelman,O.B., Vasker,I.A., Loew,G.H., Bridges,A. and Waskell,L. (1997) *Protein Eng.*, **10**, 119–129.
- Chen,J.-S., Berenbaum M.R. and Schuler,M.A. (2002) *Insect Mol. Biol.*, **11**, 175–186.
- Cohen,M.B., Berenbaum,M.R. and Schuler,M.A. (1989) *J. Chem. Ecol.*, **15**, 2347–2355.

- Cohen, M.B., Schuler, M.A. and Berenbaum, M.R. (1992) *Proc. Natl Acad. Sci. USA*, **89**, 10920–10924.
- Dai, R., Pincus, M.R. and Friedman, F.K. (2000) *Cell. Mol. Life Sci.*, **57**, 487–499.
- Domanski, T.L. and Halpert, J.R. (2001) *Curr. Drug Metab.*, **2**, 117–137.
- Domanski, T.L., Liu, J., Harlow, G.R. and Halpert, J.R. (1998) *Arch. Biochem. Biophys.*, **350**, 223–232.
- Domanski, T.L., Schultz, K.M., Roussel, F., Stevens, J.C. and Halpert, J.R. (1999) *J. Pharmacol. Exp. Ther.*, **290**, 1141–1147.
- Draper, A.J., Madan, A. and Parkinson, A. (1997) *Arch. Biochem. Biophys.*, **341**, 47–61.
- Ellis, S.W. *et al.* (1995) *J. Biol. Chem.*, **270**, 29055–29058.
- Fukuda, K., Ohta, T., Oshima, Y., Ohashi, N., Yoshikawa, M. and Yamazoe, Y. (1997) *Pharmacogenetics*, **7**, 391–396.
- Gerber, N.C. and Sligar, S.G. (1992) *J. Am. Chem. Soc.*, **114**, 8742–8743.
- Gerber, N.C. and Sligar, S.G. (1994) *J. Biol. Chem.*, **269**, 1–7.
- Gotoh, O. (1992) *J. Biol. Chem.*, **267**, 83–90.
- Graham-Lorence, S. and Peterson, J.A. (1996) *FASEB J.*, **10**, 206–214.
- Guengerich, F.P. (1997) *Adv. Pharmacol.*, **43**, 7–35.
- Guo, L.Q., Fukuda, K., Ohta, T. and Yamazoe, Y. (2000a) *Drug Metab. Dispos.*, **28**, 766–771.
- Guo, L., Taniguchi, Q.M., Xiao, Y.Q., Baba, K., Ohta, T. and Yamazoe, Y. (2000b) *Jpn J. Pharmacol.*, **82**, 122–129.
- Haining, R.L., Jones, J.P., Henne, K.R., Fisher, M.B., Koop, D.R., Trager, W.F. and Rettie, A.E. (1999) *Biochemistry*, **38**, 3285–3292.
- Halpert, J.R. and He, Y. (1993) *J. Biol. Chem.*, **268**, 4453–4457.
- Harlow, G.R. and Halpert, J.R. (1997) *J. Biol. Chem.*, **272**, 5396–5402.
- He, Y., Balfour, C.A., Kedzie, K.M. and Halpert, J.R. (1992) *Biochemistry*, **31**, 9220–9226.
- He, Y., Luo, Z., Klekotka, P.A., Burnett, V.L. and Halpert, J.R. (1994) *Biochemistry*, **33**, 4419–4424.
- He, Y.A., He, Y.Q., Szklarz, G.D. and Halpert, J.R. (1997) *Biochemistry*, **36**, 8831–8839.
- He, Y.Q., Harlow, G.R., Szklarz, G.D. and Halpert, J.R. (1998) *Arch. Biochem. Biophys.*, **350**, 333–339.
- Ho, P.C., Saville, D.J. and Wanwimolruk, S. (2001) *J. Pharm. Pharm. Sci.*, **4**, 217–227.
- Hung, C.-F., Harrison, T.L., Berenbaum, M.R. and Schuler, M.A. (1995) *Insect Mol. Biol.*, **4**, 149–160.
- Hung, C.-F., Berenbaum, M.R. and Schuler, M.A. (1997) *Insect Biochem. Mol. Biol.*, **27**, 377–385.
- Kedzie, K.M., Balfour, C.A., Escobar, G.Y., Grimm, S.W., He, Y.A., Pepperl, D.J., Regan, J.W., Stevens, J.C. and Halpert, J.R. (1991) *J. Biol. Chem.*, **266**, 22515–22521.
- Kharasch, E.D., Hankins, D.C. and Taraday, J.K. (2000) *Drug Metab. Dispos.*, **28**, 28–33.
- Kinonen, T., Pasanen, M., Gynther, J., Poso, A., Jarvinen, T., Alhava, E. and Juvonen, R.O. (1995) *Br. J. Pharmacol.*, **116**, 2625–2630.
- Kirton, S.B., Kemp, C.A., Tomkinson, N.P., St-Gallay, S. and Sutcliffe, M.J. (2002) *Proteins: Struct. Funct. Genet.*, **59**, 216–231.
- Koenigs, L.L. and Trager, W.F. (1998) *Biochemistry*, **37**, 10047–10061.
- Koenigs, L.L., Peter, R.M., Thompson, S.J., Rettie, A.E. and Trager, W.F. (1997) *Drug Metab. Dispos.*, **25**, 1407–1415.
- Lewis, D.F.V., Dickins, M., Lake, B.G., Eddershaw, P.J., Tarbit, M.H. and Goldfarb, P.S. (1999) *Toxicology*, **133**, 1–33.
- Li, H. and Poulos, T.L. (1994) *Structure*, **2**, 461–464.
- Li, H. and Poulos, T.L. (1997) *Nat. Struct. Biol.*, **4**, 140–146.
- Li, X., Berenbaum, M.R. and Schuler, M.A. (2000) *Insect Biochem. Mol. Biol.*, **30**, 75–84.
- Li, W., Petersen, R.A., Berenbaum, M.R. and Schuler, M.A. (2002a) *Insect Mol. Biol.*, **11**, 543–551.
- Li, X., Berenbaum, M.R. and Schuler, M.A. (2002b) *Insect Biochem. Mol. Biol.*, **32**, 311–320.
- Li, W., Schuler, M.A. and Berenbaum, M.R. (2003) *Proc. Natl Acad. Sci. USA*, in press.
- Lin, J.H. and Lu, A.Y.H. (1998) *Clin. Pharmacokinet.*, **35**, 361–390.
- Lindberg, R.L.P. and Negishi, M. (1989) *Nature*, **339**, 632–634.
- Lown, K.S., Bailey, D.G., Fontana, R.J., Janardan, S.K., Adair, C.H., Fortlage, L.A., Brown, M.B., Guo, W. and Watkins, P.B. (1997) *J. Clin. Invest.*, **99**, 2545–2553.
- Luo, Z., He, Y. and Halpert, J.R. (1994) *Arch. Biochem. Biophys.*, **309**, 52–57.
- Ma, R., Cohen, M.B., Berenbaum, M.R. and Schuler, M.A. (1994) *Arch. Biochem. Biophys.*, **310**, 332–340.
- MacKerell, A.D., Jr *et al.* (1998) *J. Phys. Chem.*, **102**, 3586–3616.
- Maenpaa, J., Sigusch, H., Raunio, H., Syngelma, T., Vuorela, P., Vuorela, H. and Pelkonen, O. (1993a) *Biochem. Pharmacol.*, **45**, 1035–1042.
- Maenpaa, J., Juvonen, R., Raunio, H., Rautio, A. and Pelkonen, O. (1993b) Human P450 isoform assignment by antibodies and inhibitors. PhD Dissertation, University of Oulu, Finland.
- Maenpaa, J., Juvonen, R., Raunio, H., Rautio, A. and Pelkonen, O. (1994) *Biochem. Pharmacol.*, **48**, 1363–1369.
- Martinis, S.A., Atkins, W.M., Stayton, P.S. and Sligar, S.G. (1989) *J. Am. Chem. Soc.*, **111**, 9252–9253.
- Mays, D.C., Camisa, C., Cheney, P., Pacula, C.M., Nawoot, S. and Gerber, N. (1987) *Clin. Pharmacol. Ther.*, **42**, 621–626.
- Modi, S., Paine, M.J., Sutcliffe, M.J., Lian, L.-Y., Primrose, W.U., Wolf, C.R. and Roberts, G.C.K. (1996) *Biochemistry*, **35**, 4540–4550.
- Negishi, M., Uno, T., Honkakoski, P., Sueyoshi, T., Darden, T.A. and Pedersen, L.P. (1996) *Biochimie*, **78**, 685–694.
- Omura, T. and Sato, R. (1964) *J. Biol. Chem.*, **239**, 2379–2385.
- Ono, S., Hatanaka, T., Hotta, H., Satoh, F., Gonzalez, F.J. and Tsutsui, M. (1996) *Xenobiotica*, **26**, 681–693.
- Pendurthi, U.R., Lamb, J.G., Nguyen, N., Johnson, E.F. and Tukey, R.H. (1990) *J. Biol. Chem.*, **265**, 14662–14668.
- Ravichandran, K.G., Boddupalli, S.S., Hasermann, C.A., Peterson, J.A. and Deisenhofer, J. (1993) *Science*, **261**, 731–736.
- Roussel, F., Khan, K.K. and Halpert, J.R. (2000) *Arch. Biochem. Biophys.*, **374**, 269–278.
- Ruettinger, R.T., Wen, L.-P. and Fulco, A.J. (1989) *J. Biol. Chem.*, **264**, 10987–10995.
- Rupasinghe, S., Baudry, J. and Schuler, M.A. (2003) *Prot. Eng.*, in press.
- Schmidlin-Ren, P. *et al.* (1997) *Drug Metab. Dispos.*, **25**, 1228–1233.
- Singh, J. and Thornton, J.M. (1985) *FEBS Lett.*, **191**, 1–6.
- Straub, P., Johnson, E.F. and Kemper, B. (1993) *Arch. Biochem. Biophys.*, **306**, 521–527.
- Straub, P., Lloyd, M., Johnson, E.F. and Kemper, B. (1994) *Biochemistry*, **33**, 8029–8034.
- Szklarz, G.D. and Halpert, J.R. (1997) *J. Comput. Aided Mol. Des.*, **11**, 265–272.
- Szklarz, G.D., He, Y.A. and Halpert, J.R. (1995) *Biochemistry*, **34**, 14312–14322.
- von Wachenfeldt, C. and Johnson, E.F. (1995) In Ortiz de Montellano, P.R. (ed), *Cytochrome P450: Structure, Mechanism and Biochemistry*, 2nd edn. Plenum Press, New York, pp. 183–223.
- Wang, H., Dick, R., Yin, H., Licad-Coles, E., Kroetz, D.L., Szklarz, G., Harlow, G., Halpert, J.R. and Correia, M.A. (1998) *Biochemistry*, **37**, 12536–12545.
- Williams, P.A., Cosme, J., Sridhar, V., Johnson, E.F. and McRee, D.E. (2000) *Mol. Cell*, **5**, 121–131.
- Zhang, W., Kilicarslan, T., Tyndale, R.F. and Sellers, E.M. (2001) *Drug Metab. Dispos.*, **26**, 897–902.

Received December 4, 2002; revised June 8, 2003; accepted June 23, 2003